J Solid State Electrochem (2007) 11:719–726
DOI 10.1007/s10008-007-0284-6

ORIGINAL PAPER

ZnO thin films electrodeposited in propylene carbonate under a magnetic field

M. Morisue · M. Nambu · H. Osaki · Y. Fukunaka

Received: 4 June 2006 / Revised: 15 January 2007 / Accepted: 5 February 2007 / Published online: 23 March 2007

Abstract Electrochemical processing of ZnO films on fluorine-doped indium tin oxide (FTO/ITO) substrate was investigated in organic propylene carbonate electrolyte solutions containing $Zn(NO_3)_2{\cdot}6H_2O$. Much finer and more uniform morphologies of the ZnO films were obtained in comparison with those in aqueous electrolyte solutions. The effects of superimposing a magnetic field to the ZnO films were further examined. Superimposing a magnetic field considerably influenced the transient current density in the initial stage, especially in the mass transfer controlled region at −1.5 V vs Zn wire reference electrode. It also introduced substantially no drastic influence on the microstructure in spite of the appearance of considerably significant morphological variations.

Introduction

The electrical, optical, and acoustic characteristics of zinc oxide have been of considerable interest. It is widely applied to chemical sensors, liquid crystal display, transparent conductive film, blue light-emitting diode, catalysis, and others [1–5]. ZnO films are also of technological importance as nanoporous films for dye-sensitized solar cells [6].

ZnO is normally an n-type semiconductor with a room temperature band gap of 3.2 eV. Although the stoichiometric ZnO film is highly resistive, a conducting film can be manufactured either by introducing oxygen vacancies, which act as donors or by doping with Al, Ga, or In. Various doping strategies have been introduced to prepare p-type ZnO [7–9].

In general, ZnO films can be deposited onto a substrate via pulsed laser deposition [10], sputtering [11], gas phase deposition [12], metal organic chemical vapor deposition [13], molecular beam epitaxy [14, 15], and spray pyrolysis [16]. Solution methods such as sol-gel synthesis [17], chemical solution precipitation [18], hydrothermal synthesis [19], anodic oxidation [20], and electrodeposition have also been reported.

Electrochemical deposition of ZnO films from aqueous solution has been described by Izaki et al. [21–25] and Peulon et al. [26–29]. The former used a nitrate solution by simultaneously reducing dissolved oxygen as NO_3^- source in the deposited film, whereas the latter employed a chloride bath with O_2 gas bubbling. Many papers have been reported on the electrodeposition of ZnO/dye hybrid films for dye-sensitized solar cell [30–40].

Cathodic deposition of ZnO has also been reported from nonaqueous solution such as dimethyl sulfoxide [41, 42] and propylene carbonate (PC) [43, 44]. ZnO films electrodeposited in nonaqueous baths may be different in many ways from those deposited in aqueous solutions. Higher deposition temperature can be used, usually leading to better crystallinity and larger crystal sizes of the deposits. The surface morphology and crystalline structure of ZnO may be more easily controlled by electrodeposition in nonaqueous solution.

During the recent years, high magnetic fields have become readily available owing to the rapid advance in both permanent magnets and superconducting magnets. Magnetic fields have been applied to the electrochemical processing of tailored materials [45]. In high magnetic fields, new phenomena caused by the Lorentz forces as well

Contribution to special issue on Magnetic field effects in Electrochemistry.

M. Morisue · M. Nambu · H. Osaki · Y. Fukunaka (✉)
Department of Energy Science and Technology, Kyoto University, Kyoto, Japan
e-mail: fukunaka@energy.kyoto-u.ac.jp

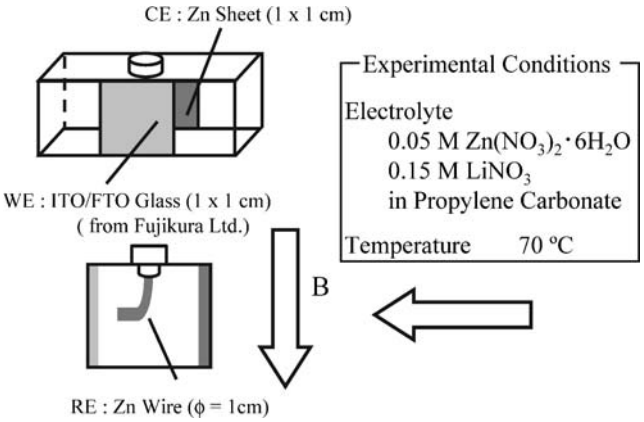

Fig. 1 Schematic illustration of electrolytic cell

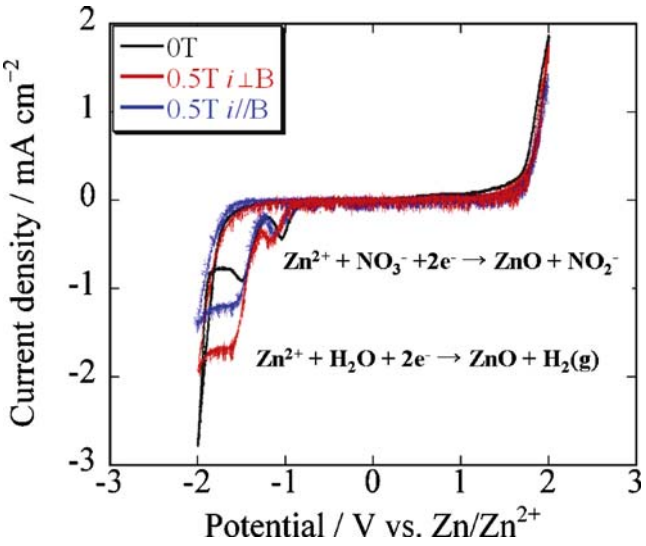

Fig. 3 Cyclic voltammograms in PC electrolyte (10 mV/sec)

as by the magnetization forces are expected. Moreover, various magnetic effects become tangible not only in ferromagnetic materials but also nonmagnetic ones such as paramagnetic and diamagnetic, on which the effect of a magnetic field has been considered to be negligible hitherto.

Oxide films like ZnO have characteristic anisotropies with crystal orientation that induce various unique electro-optical functions [46, 47]. It is indispensable for the device application to control the oxide film orientation. There are yet few reports about the orientation control of ZnO thin films prepared by electrochemical depositions under a magnetic field. The main subject of this study is to find out effects caused by superimposing a magnetic field on ZnO films electrodeposited in PC electrolyte. Magnetic field effects on the surface morphology and microcrystalline variations are investigated.

Experimental

ZnO films were electrodeposited onto transparent conductive glass substrates (fluorine-doped indium tin oxide FTO/ITO) coated glass, 2 Ω/cm, Fujikura). Before electrodeposition, the substrates were ultrasonically cleaned sequentially in acetone, ethanol, and deionized water for 15 min, respectively. They were additionally soaked in trichloroethylene for 3 min and rinsed in deionized water.

Electrochemical experiments were carried out with a conventional three-electrode system as illustrated in Figure 1. The electrode assembly was composed of a short rectangular channel (10×10×30 mm, Teflon) with two open ends and was immersed in a 50 ml electrolyte solution bath. The counter electrode was a zinc sheet (Nilaco). The effective surface area of both electrodes was 10×10 mm^2. They were embedded in either side of channel walls. A Zn wire (ϕ=1 mm, Nilaco) was used as a conventional reference electrode.

ZnO was electrodeposited from PC electrolyte containing 0.05 M $Zn(NO_3)_2{\cdot}6H_2O$ and 0.15 M $LiNO_3$ at 343 K. Karl–Fischer titration was used to measure water content in the PC electrolyte. Experiments were conducted by using a potentiostat/galvanostat (Hokuto Denko) and a function generator (Hokuto Denko). The amount of electricity was controlled by a coulomb meter (Hokuto Denko).

The electrodeposited films were soaked twice in acetone for 20 min. After rinsing again in acetone, they were dried

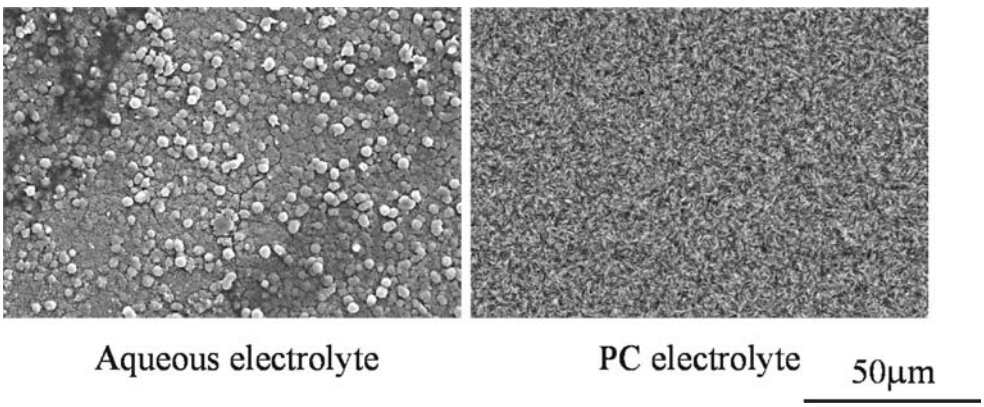

Fig. 2 SEM images of ZnO electrodeposited in aqueous and PC electrolyte containing 0.1 M $Zn(NO_3)_2{\cdot}6H_2O$

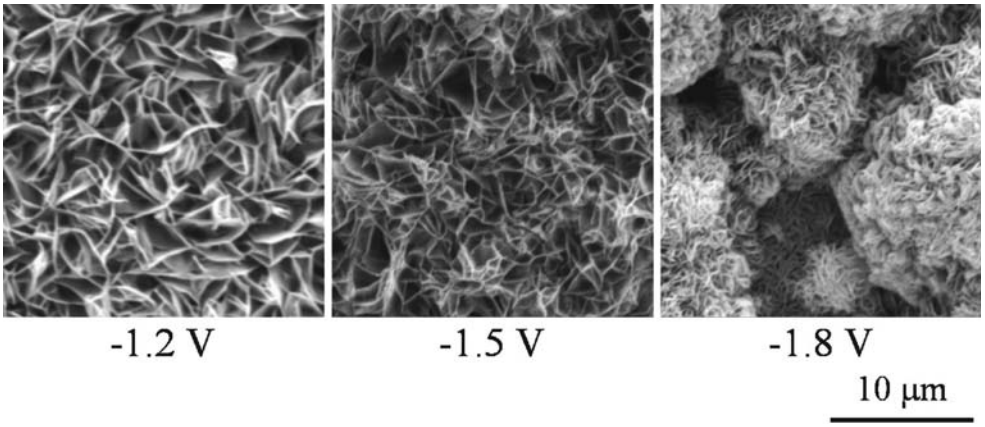

Fig. 4 SEM images of electrodeposited ZnO from PC electrolyte containing 0.05 M $Zn(NO_3)_2{\cdot}6H_2O$ and 0.15 M $LiNO_3$

in an air stream. The surface morphology of the electrodeposited ZnO film was observed by scanning electron microscopy (SEM; S-2600H, Hitachi) and atomic force microscopy (AFM; SPI3800, Seiko Instruments). The preferred crystal orientation of the electrodeposited films was analyzed by X-ray crystallography (XRD) for thin film using Cu-Kα line (X'Pert, Philips, 40 kV, 40 mA).

A permanent Nd–Fe–B magnet of 0.5 T was used to induce a static and uniform magnetic field that is parallel or perpendicular to the substrate surface.

Results and discussion

Electrodeposition in PC electrolyte

Before starting the electrochemical processing in the PC electrolyte, ZnO films were electrodeposited in aqueous solution containing the same amount of $Zn(NO_3)_2{\cdot}6H_2O$ as that of the PC electrolyte. The equilibrium electrochemical reaction cannot be clearly defined at the interface between the conventional Zn reference electrode and PC electrolyte. Nevertheless, the surface morphology of ZnO precipitated in the aqueous system is barely comparable with that from the PC solution as long as the oxide films were precipitated at apparently the same electrode potential of −1.2 V vs Zn wire conventional reference electrode. Figure 2 illustrates a finer and more uniform surface morphology in the PC electrolyte. The current density of 2 mA/cm^2 recorded in aqueous solution is considerably higher than that in PC electrolyte. When the morphology precipitated at almost same current density is compared in both electrolyte solutions, much finer or bamboo-leaf-like precipitates are obtained, and a higher anisotropic growth is observed in the PC solution. That is, more degree of freedom to control the morphological variations is possible in the PC electrolyte. These facts motivated us to further examine the electrochemical processing of ZnO films in PC electrolytes.

In this study, $Zn(NO_3)_2{\cdot}6H_2O$ is used as a solute component in organic PC solution. When all hydration water associated with zinc nitrate salt is dissolved in PC, the water content attains 0.44%. Nishikawa et al. [49] measured the increase in H_2O concentration to 200 ppm during the holographic interferometry measurement of Li^+ ion concentration profile associated with Li electrodeposition in PC electrolyte [48]. It is thus deduced that the H_2O contamination from the atmosphere will be negligible. In the PC electrolyte, chemical species like Zn^{2+}, NO_3^-, and H_2O are participating complicatedly to the electrodeposition reaction of ZnO. In a series of research, cyclic voltammetry (CV) was applied for various compositions

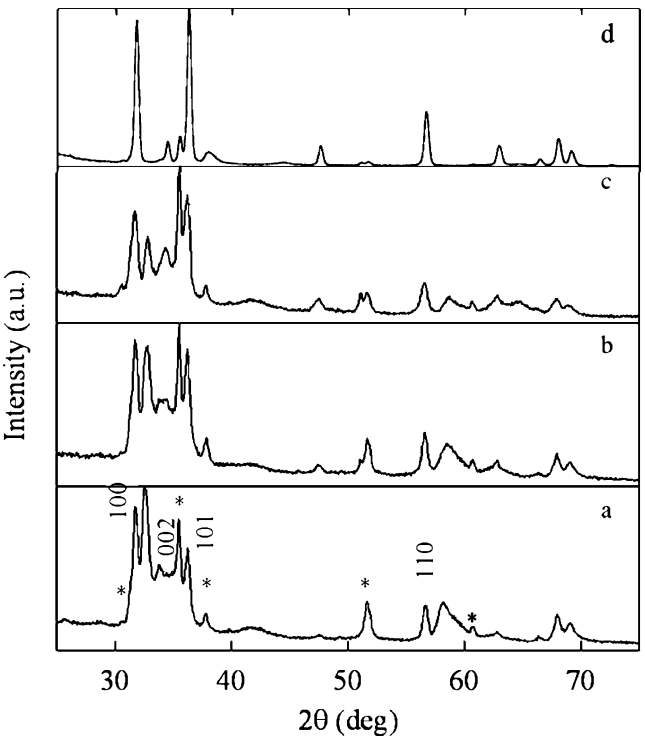

Fig. 5 XRD spectra of ZnO electrodeposited from PC electrolyte containing 0.05 M $Zn(NO_3)_2$ and 0.15 M $LiNO_3$. **a** −1.2 V, **b** −1.5 V, **c** −1.8 V, **d** −1.8 V and annealed

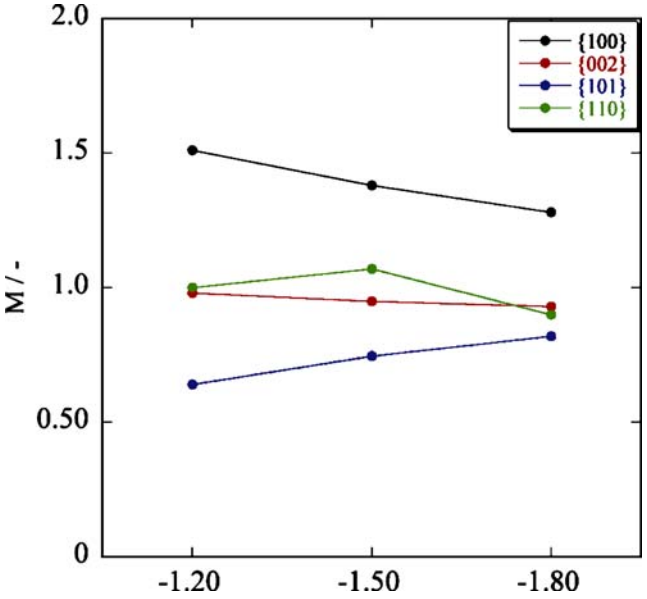

Fig. 6 Orientation index of ZnO electrodeposited in PC electrolyte containing 0.05 M $Zn(NO_3)_2{\cdot}6H_2O$, 0.15 M $LiNO_3$

of PC electrolytes [50]. The peak potential or peak current shifted with the variation of Zn^{2+} and H_2O concentration.

In aqueous electrolyte solution systems, a general scheme of electroprecipitation of ZnO films from nitrate bath has been proposed as follows [35]. Electroreduction in nitrate ions generates hydroxide ions at the cathode as expressed by

$$NO_3^- + H_2O + 2e^- \rightarrow NO_2^- + 2OH^- \qquad E^0 = +0.1\,V \tag{1}$$

Zinc ions react with the hydroxyl anions to precipitate zinc hydroxide. It is rapidly dehydrated into ZnO at higher temperatures.

$$Zn^{2+} + 2OH^- \rightarrow Zn(OH)_2 \rightarrow ZnO + H_2O \tag{2}$$

The overall expression of oxide electrodeposition reaction therefore is written as,

$$Zn^{2+} + NO_3^- + 2e^- \rightarrow ZnO + NO_2^- \tag{3}$$

Moreover, the cathodic current starts to increase again at more negative potential, which may be described by Eq. 4.

$$2H_2O + 2e^- \rightarrow H_2 + 2OH^- \tag{4}$$

This reaction may be expected even in PC electrolyte, because a certain amount of H_2O is inevitably introduced. It is then expected that Eq. 4 is followed by

$$Zn^{2+} + H_2O + 2e \rightarrow ZnO + H_2(g) \tag{5}$$

When the electrolysis is started with a vertical electrode installed in a stagnant electrolyte, it is expected that an upward natural convection is induced along the vertical cathode associated with the cathodic reaction (3). At the same time, Zn metal electrochemically dissolves into aqueous electrolyte as Zn^{2+} ion to induce a downward natural convection along an anode surface. The induction of natural convection caused by the electrochemical reaction has been reasonably analyzed based on the boundary layer theory in aqueous solution system, as long as the electrode reaction does not accompany any gas bubble evolution or passivation phenomena [51, 52].

Figure 3 (0T) demonstrates an example of CV results measured at the sweep rate of 10 mV/s in PC electrolyte. The cathodic current peak around −1.5 V was apparently affected by zinc concentration (Nambu et al., to be submitted). When the cathodic current is controlled by the mass transfer rate of Zn^{2+} ion toward the cathode surface immersed in PC electrolyte, a simple materials balance equation provides the limiting current density concept. An effective boundary layer thickness of 400 ìm gives a limiting current density of about 1 mA/cm^2, which is close to the observed value in Fig. 3. The effective boundary

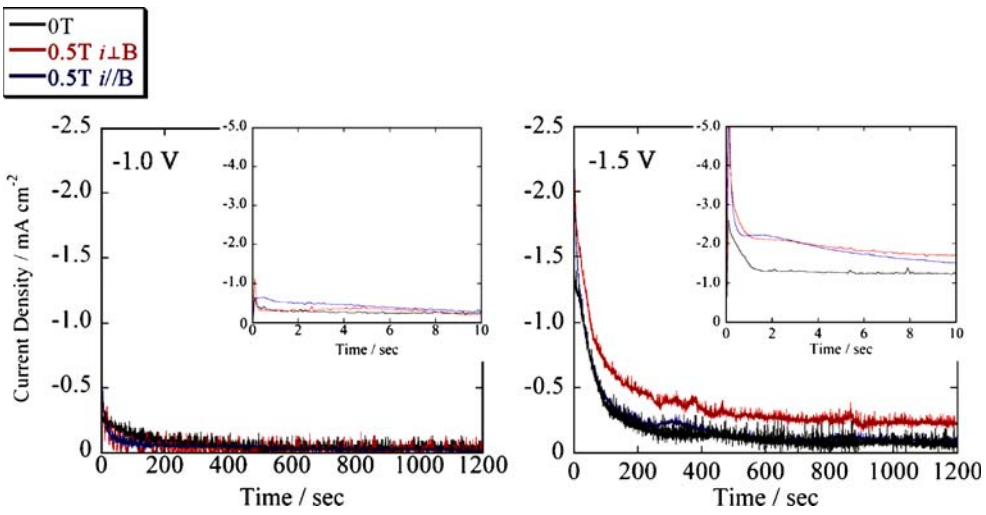

Fig. 7 Transient behavior of current density

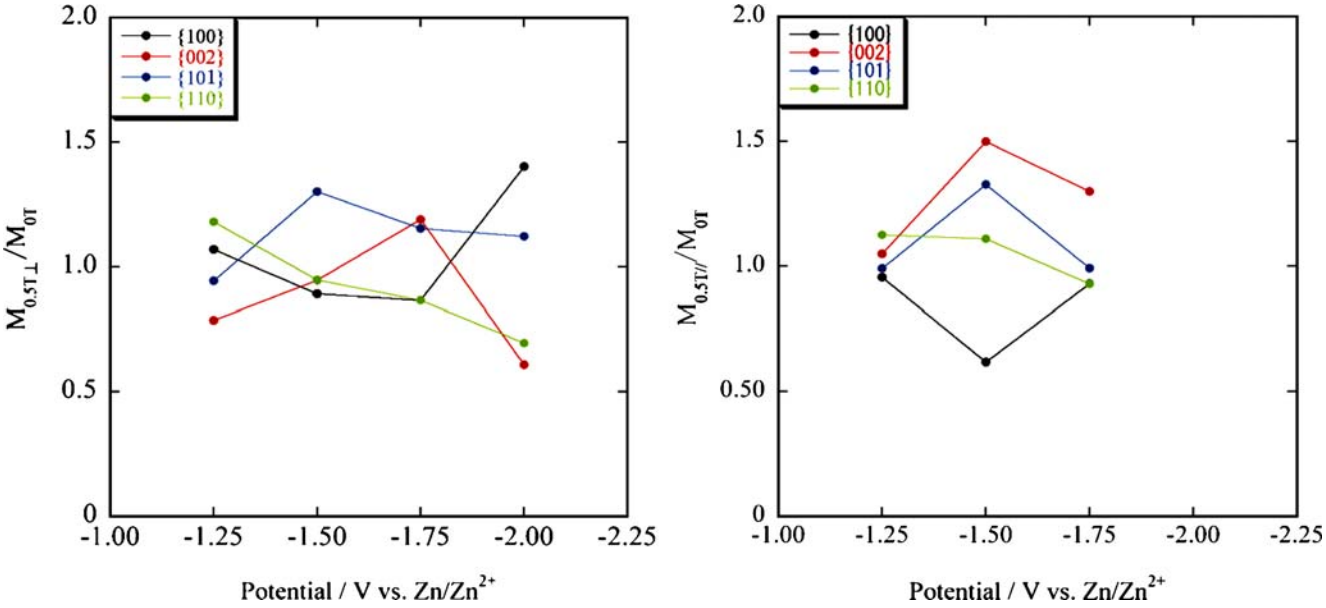

Fig. 8 Relationship between orientation index ratio and electrode potential (*left*: perpendicular, *right*: parallel)

layer thickness is now in situ measured with a holographic interferometer at the Kyoto University [50].

The surface pH value rises significantly by the competitive electrochemical reactions between Eqs. 1 and 4 at the lower electrode potential region even in PC electrolyte. It is reasonable to assume intermediate precipitations of Zn $(OH)_2$ on the substrate surface. When the electrodeposition is performed at an elevated temperature, $Zn(OH)_2$ is rapidly converted to ZnO during electrodeposition.

In consequence, the electrochemical deposition of ZnO is possible even in nonaqueous solution. $Zn(OH)_2$ more significantly precipitates with increasing H_2O concentration. When H_2O molecules are not present in the PC electrolyte, the deposition rate becomes very slow, and Zn metal deposition is expected. It seems that an optimum H_2O content exists in PC electrolytes for the deposition of ZnO. The details of the CV measurements are described in a separate paper (Nambu et al., to be submitted).

Characterization of ZnO film electrodeposited in PC electrolyte

ZnO thin films are potentiostatically electrodeposited to examine the effect of electrode potential on the surface morphology and microstructure variations of the deposited films. Figure 4 shows SEM images of ZnO films deposited in PC solutions at −1.2, −1.5, and −1.8 V, respectively. The averaged current density recorded at each potential is 0.2, 0.9–1.0, and 1.0 mA/cm^2, respectively. The total electrical charge is restricted to 2.0 C/cm^2. In this condition, no zinc

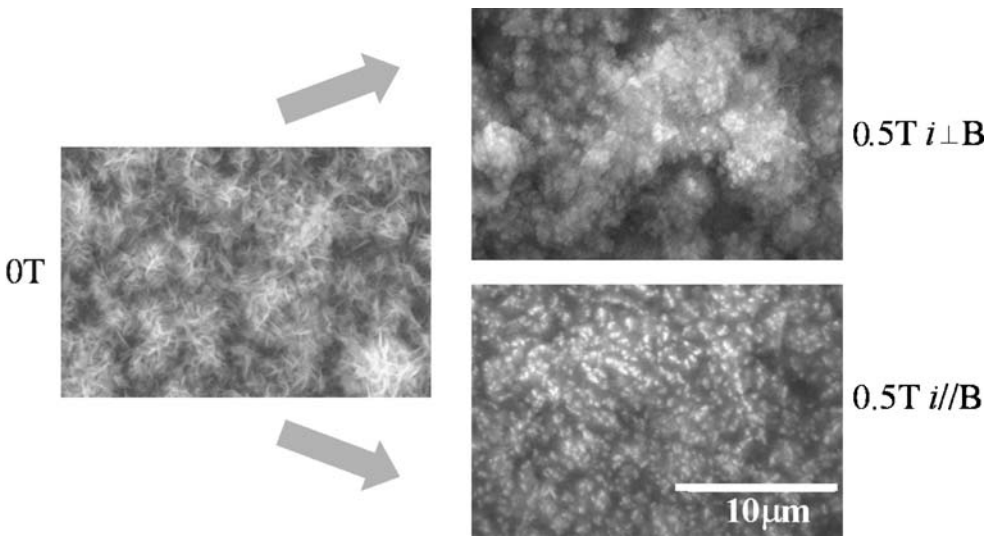

Fig. 9 SEM images of ZnO thin films electrodeposited with and without magnetic field

metal is deposited. The size of bamboo-leaf-like precipitates uniformly grown on the substrate becomes smaller with decreasing deposition potential. The film deposited at −1.8 V shows a coagulation mode of finer precipitates to result in an apparently macroscopic spherical deposit 10 μm in size.

XRD spectra for these three films as deposited are shown in Fig. 5. The peak marked with an asterisk symbol stems from the FTO/ITO substrate. Diffraction patterns corresponding to (100) and (101) planes of wurtzite ZnO are noticed although all peaks are very low and broad. The peak for the (002) plane is almost hidden in the background spectra at −1.2 V and becomes visible with decreasing potential.

The reduction rate of the NO_3^- or H_2O molecules reaches the limiting current density below −1.5 V. It is deduced that only Eq. 3 or 5 are substantially driven at more negative potential to result in the electrochemical formation of ZnO. Four peaks of the (100), (002), (101), and (110) planes are clearly identified for ZnO films annealed at 400 °C (Fig. 5d). The detailed results are described elsewhere [50].

To evaluate the preferred orientation parallel to the substrate plane, the orientation index M was calculated as follows,

$$M(hkl) = \frac{\frac{I(hkl)}{\sum I(h'k'l')}}{\frac{I_0(hkl)}{\sum I_0(h'k'l')}} \quad (6)$$

where $I(hkl)$ is the XRD intensity of the experimental data, $I_0(hkl)$ is the intensity reported in the JCPDS cards. $\sum I(h'k'l')$ in the present case is the sum of the intensities of four independent peaks: (100), (002), (101), (110). The orientation index $M(hkl)$ is calculated from Eq. 6. If all the crystal planes would be orientated in all directions with the same probability as those in the powder pattern, the M values of the crystal planes should be equal to unity. $M>1$ and <1 indicate a more preferential and more suppressed orientation of the (hkl) plane towards the surface than $M=1$, respectively.

Figure 6 shows the dependence of the electrode potential for the orientation index M of electrodeposited ZnO films in Fig. 4. The (100) plane, which has the most stable characteristics, is slightly preferably oriented, and (101) is suppressed, whereas (002) and (110) are located close to that of the powder pattern at −1.2 V. Such a difference between the M values for the (100) and (101) plane becomes smaller and approach the powder pattern with decreasing electrode potential.

Electrodeposition of ZnO under a magnetic field

The magnetohydrodynamic (MHD) effect is caused by the Lorentz force,

$$F_L = j \times B$$

where j is the current density, B is the applied magnetic field, and F is the Lorentz force. This force acts on the moving ions in the electrolyte solution, resulting in convective flow of the organic electrolyte. F_L is a uniform magnetic body force acting on a volume element of solution. When the electric flux crosses the magnetic flux horizontally, a MHD convective flow is introduced vertically. The ionic mass transfer near the cathode is enhanced, while the downward natural convection along an anode is disturbed by the upward MHD convection. The cathode current density for the deposition of ZnO film becomes higher than that without a magnetic field. As the current density decreases, the contribution of the MHD effect to the ionic mass transfer rate becomes smaller.

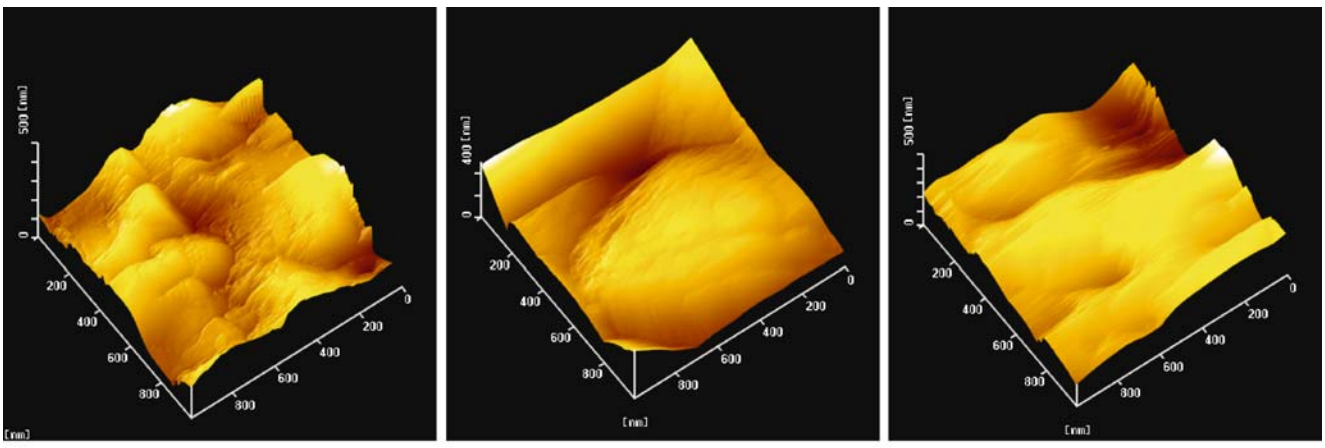

Fig. 10 AFM images of ZnO film electrodeposited under magnetic field (*Left*: OT, *middle*: perpendicular, *right*: parallel)

The magnetic field of the Nd–Fe–B permanent magnet was superimposed perpendicular and parallel to the electrical field. Figure 3 shows the cyclic voltammograms measured in the PC electrolyte at 343 K, with and without a magnetic field of 0.5 T. No essential difference between 0 and 0.5 T is recognized around −1.0 V. The current density is, however, significantly enhanced below −1.5 V irrespective of the direction of the superimposed field. Obviously, the MHD convection enhances the ionic mass transfer rate of the Zn^{2+} and NO_3^- ions towards the substrate for the perpendicular direction.

The transient current density variations at −1.0 V and −1.5 V over 1,200 s are demonstrated in Fig. 7. The superposition effect of the magnetic field is covered by the fluctuation of the current transient at −1.0 V, while it becomes evident for the perpendicular field at −1.5 V. It is more clearly noticed in the insets, in which the time unit is magnified over the initial 10 s. Just after the electrolysis is started, not only a perpendicular but also a parallel magnetic field at −1.5 V considerably enhances the transient current density. The parallel field may become effective because of the nonuniform electric field between both electrodes. The reason why such a magnetic field superimposition effect significantly appears at the beginning of electrodeposition must be studied, because it is indispensably coupled with the electrodics of Eq. 1 or 4.

The ratio of M in a magnetic field to that without magnetic field, $M_{0.5T}/M_{0T}$ plotted against the potential in Fig. 8. Each plane demonstrates a characteristic variation with decreasing potential irrespective of the direction of the superimposed magnetic field, although the degree of variation is not so significant. Pole figure measurements may provide more positive evidence.

Figure 9, on the other hand, demonstrates the morphological variation of a ZnO film electrodeposited at −1.5 V in a perpendicular and a parallel magnetic field of 0.5 T. The bamboo-leaf-like deposit drastically turns to roundish precipitates under the superimposed magnetic field. The perpendicular field introduces finer precipitates coagulated with each other, while coarser grains with submicron meter size are observed in parallel fields. AFM images are shown in Fig. 10. They would support a possible influence through the ionic mass transfer rate because of magnetic field on the morphology of electrodeposited film, if the morphological variation would be quantitatively measured with AFM technique.

Summary

ZnO films were electrodeposited on FTO/ITO substrates in PC electrolyte solutions containing $Zn(NO_3)_2{\cdot}6H_2O$. CV measurements suggested an electrodeposition mechanism for the ZnO films in which H_2O molecules are indirectly participating. ZnO films were further electrodeposited under a magnetic field. The transient current density in the initial stage over a few seconds superimposed by a magnetic field was significantly enhanced in the mass transfer controlled region at −1.5 V. It is noteworthy to describe that the superimposition of a magnetic field to the electrical field introduces substantially no drastic influence on the microstructure in spite of the morphological variation clearly demonstrated in Fig. 9. Scaling factor analysis is necessary to clarify the quantitative effect of magnetic field on the morphological variation.

Acknowledgments Part of this work was performed under the financial aid given to Y. F. by the Ministry of Education, Science and Technology (Project no. 15360402), and Kyoto University COE program (Establishment of COE on Sustainable Energy System) for which the authors are grateful. The author wish to thank Drs. T. Iida, T. Kitamura, K. Nishikawa and Mr. K. Goto for their constant support on this study.

Reference

1. Nanto H, Tsubakino S, Kawai T, Ikeda M, Kitagawa S, Habara M (1994) J Mater Sci 29:6529
2. Muller J, Weissenrieder S, Fresenius J (1994) Anal Chem 349:390
3. Iwata K, Sakemi T, Yamada A, Fons P, Awai K, Yamamoto T, Matsubara M, Tampo H, Sakurai K, Ishizuka S, Niki S (2004) Thin Solid Films 451:219
4. Tsukazaki A, Ohtomo A, Onuma T, Ohtani M, Makino T, Sumiya M, Ohtani K, Chichibu SF, Fuke S, Segawa Y, Ohno H, Koinuma H, Kawasaki M (2005) Nature Mat 4:42
5. Jacobs H, Mokwa W, Kohl D, Heiland G (1985) Surf Sci 160:217
6. O'Regan B, Grätzel M (1991) Nature 353:737
7. Lee EC, Chang KJ (2004) Phys Rev B 70:115210
8. Kurimoto M, Almamun Ashrafi ABM, Ebihara M, Uesugi K, Kumano H, Suemune I (2004) Phys Stat Solidi B 241:635
9. Ryu YR, Zhu S, Look DC, Wrobel JM, Jeong HM, White HW (2000) J Cryst Growth 216:330
10. Zeng JN, Low JK, Ren ZM, Liew T, Lu YF (2002) Appl Surf Sci 197:362
11. Sen S, Leary DJ, Bauer CL (1982) Thin Solid Films 94:7
12. Goossens A, Maloney EL, Schoonman J (1998) Chem Vap Depos 4:109
13. Vanheusden K, Seager CH (1996) l Appl Phys Lett 68:4034
14. Chen Y, Bagnall DM, Zhu Z, Sekiuchi T, Park K, Hiraga K, Yao T, Koyama S, Shen MY, Goto T (1997) J Cryst Growth 181:165
15. Segawa Y, Ohtomo A, Kawasaki M, Koinuma H, Tang ZK, Yu P, Wong GK (1997) Phys Stat Solidi B 202:669
16. Vanheusden K, Seager CH, Warren WL, Tallant DR, Caruso J, Hapmden-Smith MJ, Kodas TT (1997) J Luminescence 75:11
17. Tang W, Cameron DC (1994) Thin Solid Films 238:83
18. Niesen TP, De Guire MR (2001) J Electroceram 6:169
19. Yamabi S, Imai H (2002) J Mater Chem 12:3773
20. Sato Y, Shindo T, Iizuka H, Taguchi H, Ogasawara T, Sato S (1998) J Ceram Soc Jpn 106 (2):231
21. Izaki M, Omi T (1996) Appl Phys Lett 68:2437
22. Izaki M, Omi T (1996) J Electrochem Soc 143:L53
23. Izaki M, Katayama J (2000) J Electrochem Soc 147:210
24. Ishizaki H, Izaki M, Ito T (2001) J Electrochem Soc 148:C540
25. Ishizaki H, Imaizumi M, Matsuda S, Izaki M, Ito T (2002) Thin Solid Films 411:65

26. Peulon S, Lincot D (1996) Adv Mater 8:166
27. Peulon S, Lincot D (1998) J Electrochem Soc 145:864
28. Pauporte T, Lincot D (1999) Appl Phys Lett 75:3817
29. Pauporte T, Cortes R, Froment M, Beaumont B, Lincot D (2002) Chem Mater 14:4702
30. Yoshida T, Tochimoto M, Schlettwein D, Wöhrle D, Sugiura T, Minoura H (1999) Chem Mater 11:2657
31. Yoshida T, Terada K, Schettwein D, Oekermann T, Sugiura T, Minoura H (2000) Adv Mater 12:1214
32. Yoshida T, Minoura H (2000) Adv Mater 12:1219
33. Yoshida T, Pauporté T, Lincot D, Oekermann T, Minoura H (2003) J Electrochem Soc 150:C608
34. Oekermann T, Karuppuchamy S, Yoshida T, Schettwein D, Wöhrle D, Minoura H (2004) J Electrochem Soc 151:C62
35. Yoshida T, Kamatsu D, Shimokawa N, Minoura H (2004) Thin Solid Films 451–452:166
36. Gu ZH, Fahidy TZ (1999) J Electrochem Soc 146:156
37. Nomura K, Shibata N, Maeda M (2002) J Cryst Growth 235:224
38. Dalchiele EA, Giorgi P, Marotti RE, Martín F, Ramos-Barrado JR, Ayouci R, Leinen D (2001) Sol Energy Mater Sol Cells 70:245
39. Marotti RE, Guerra DN, Bello C, Machado G, Dalchiele EA (2004) Sol Energy Mater Sol Cells 82:85
40. Konenkamp R, Boedecker K, Lux-Steiner MC, Poschenrieder M, Zenia F, Levy-Clement C, Wagner S (2000) Appl Phys Lett 77:2575
41. Gal D, Hodes G, lincot D, Schock H-W (2000) Thin Solid Films 361–362:79
42. Jayakrishnan R, Hodes G (2003) Thin Solid Films 440:19
43. O'Regan B, Schwartz DT, Zakeeruddin SM, Grätzel M (2000) Adv Mater 12:1263
44. O'Regan B, Sklover V, Grätzel M (2001) J Electrochem Soc 148: C498
45. Bodea S, Ballou R, Molho P (2004) Phys Rev E 69:021605
46. Minami T, Nanto H, Sato H, Takeda S (1988) Thin Solid Film 164:275
47. Sakka Y, Suzuki TS (2005) J Ceram Soc Jpn 113:26
48. Ota M, Izuo S, Nishikawa K, Fukunaka Y, Kusaka E, Ishii R, Selman JR (2003) J Electroanal Chem 559:175
49. Nishikawa K, Ota M, Izuo S, Fukunaka Y, Kusaka E, Ishii R, Selman JR (2004) J Solid State Electrochem 8:174
50. Nambu M (2005) Master thesis, Kyoto University
51. Denpo K, Okumura T, Fukunaka Y, Kondo Y (1985) J Electrochem Soc 132:1145
52. Fukunaka Y, Nakamura Y, Konishi Y (1998) J Electrochem Soc 145:3814